Available on CMS information server

CMS NOTE 2006/129

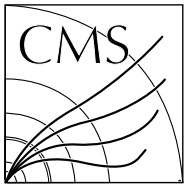

The Compact Muon Solenoid Experiment

CMS Note

Mailing address: CMS CERN, CH-1211 GENEVA 23, Switzerland

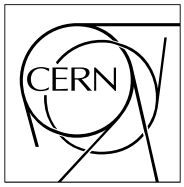

June 17, 2006

Search for ADD direct graviton emission in photon plus missing transverse energy final state at CMS

J.Weng

CERN, Geneva, Switzerland & University of Karlsruhe, Germany

G. Quast, C. Saout

University of Karlsruhe, Germany

A. De Roeck, M. Spiropulu

CERN, Geneva, Switzerland

Abstract

The exclusive γ and $\not\!\!E_T$ signature is used as a probe for the discovery reach of ADD large extra dimensions at the CMS detector. Signal samples for various model parameters as well as possible backgrounds have been simulated using the CMS fast detector simulation. The reconstruction performance and efficiency obtained with the fast simulation has been compared in detail with full simulation. A normalisation method is proposed to measure the main background $Z^0(\rightarrow \nu\bar{\nu}) + \gamma$ with high precision using reference spectra from $Z^0(\rightarrow \mu^+\mu^-) + \gamma$ and $Z^0(\rightarrow e^+e^-) + \gamma$. The discovery reach at the LHC with CMS is presented and the potential to determine parameters of the underlying model is discussed.

1 Introduction

In recent years there has been an increasing interest in models that introduce extra dimensions in addition to the 3+1 dimensions from everyday's experience, in order to solve the hierarchy problem in particle physics. The extra dimensions scenario of Arkani-Hamed, Dvali, and Dimopoulos [ADD] [12] was the first extra dimensions model in which the compactified dimensions can be of macroscopic size, but stay consistent with all current experiments and observations; they are therefore referred to as "large extra dimensions" models. In these models, new physics can appear at a mass scale of the order of 1 TeV and can therefore be accessible at LHC. In the most basic version, n extra spatial dimensions are compactified on a torus with common circumference R, and a brane is introduced which extends only in the three infinite spatial directions. The additional dimensions must be compactified on some scale R so that they are currently unobserved. Strictly speaking, the brane should have a very small tension (energy per unit volume) in order that it does not significantly warp the extra dimensional space. It is assumed that all standard model fields can extend only in the brane.

A consequence of these assumptions is that the effective 4d Planck scale is related to the underlying fundamental Planck scale of the $4+n$-dimensional theory and to the volume of the compactified space. This relation follows from Gauss' Law or by dimensional truncation:

$$M_{\mathrm{Planck}}^2 = M_D^{2+n}\, R^n \quad , \tag{1}$$

where M_{Planck}^2 is defined by Newton's constant: $M_{\mathrm{Planck}} = 1/\sqrt{G_N} = 1.2 \times 10^{19}$ GeV. M_D^{2+n} is defined as the gravitational coupling which appears in the $4+n$-dimensional version of the Einstein-Hilbert action. It is the quantum gravity scale of the higher dimensional theory. One of the shortcomings of the standard model of particle physics is the lack of an explanation for the large hierarchy of scales that exists between the mass scale of the weak interaction, set by the Fermi constant G_F (or the W-mass, M_W) and that of gravity, set by Newtons constant G_N. If M_{Planck}, M_D and $1/R$ in Eq. 1 are all of the same order, as is usually assumed in string theory, this relation is not very interesting, since new physics would not be visible until these huge energy scales are reached. But it is plausible and experimentally allowed that M_D is equal to a completely different scale. It has been suggested in the ADD model that R could be much larger, allowing the fundamental scale of gravity to be close to M_W and thus remove the large hierarchy of scales and render observations of quantum gravity at the LHC plausible. In this picture the apparent weakness of observed gravity is due to its dilution by spreading of its field into the additional dimensions. However, it should be noted that the hierarchy problem is translated from an ultraviolet to an infrared problem.

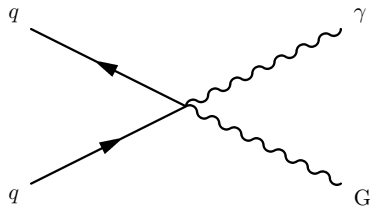

Figure 1: Feynman graph of the ADD Graviton production together with a photon

When an extra dimension is compactified on a circle with size R, particles propagating into the extra dimensions appear, from a four-dimensional viewpoint, as a tower of states. In the ADD model only the gravitons probe the full bulk space. There is therefore a Kaluza-Klein tower of graviton modes, where the massless mode is the standard 4d graviton, and the other KK modes are massive spin 2 particles which also couple to SM matter with gravitational strength. Gravitons propagating in the extra dimensions will appear to be massive. Whereas bremsstrahlung of ordinary gravitons is a completely negligible effect at colliders, the total cross section to produce *some* massive KK graviton is volume enhanced, and effectively suppressed only by powers of M_D and not M_{Planck}. From Eq. 1 it follows:

$$\sigma \sim \frac{1}{M_{\mathrm{Planck}}^2}(ER)^n \sim \frac{1}{M_D^2}(EM_D)^n \tag{2}$$

where E is the characteristic energy of the subprocess. The relevant processes for the LHC are $gg \to gG$, $qg \to qG$ and $q\bar{q} \to Gg$ which give rise to final states of jets plus missing transverse energy. The other significant contribution to the Graviton production is the $q\bar{q} \to G\gamma$ process, which leads to an experimental signature of a photon plus $\not{E}_T$ and is studied in this note; the Feynman graph of the processes is show in 1, the cross section are given in [4].

1.1 Previous results and limits for the ADD scenario

For the two parameters of the ADD model, the fundamental scale $\mathrm{M_D}$ and the number of extra dimensions n, some constraints already exist. The case $n = 1$ is already excluded since it would imply deviations of the Newton law of gravitational attraction at distance scales that have already been explored. Due to the decreasing cross section for graviton emission a scenario with $n > 6$ is very hard to detect at the LHC and has not been studied in this analysis. The lower value of M_D should be larger than the current direct limit - the limits published by LEP can be seen in table 1.

$e^+e^- \rightarrow \gamma\mathrm{G}$					
	$n = 2$	$n = 3$	$n = 4$	$n = 5$	$n = 6$
Aleph	1.28	0.97	0.78	0.66	0.57
Delphi	1.38	1.02	0.84	0.68	0.58
L3	1.02	0.81	0.67	0.58	0.51

Table 1: Combined limits on $\mathrm{M_D}$ (in TeV) from LEP.

Furthermore, the low $\mathrm{M_D}$ region should be considered with some care: here one has significant contributions from events where the partonic centre-of-mass energy is higher than $\mathrm{M_D}$, which is a not appropriate, as discussed in the analysis section.

2 Studies of the model at generator level

The topology of the single photon + graviton event can be characterised by:

- a single high p_T photon in the central η region
- high missing p_T back to back to the photon in the azimuthal plane with a similar p_T distribution.

These characteristics listed above are almost independent of the parameters and shown in figure 2 for an ADD scenario with two extra dimensions ($n = 2$) and a fundamental scale $\mathrm{M_D} = 5\ \mathrm{TeV}$. In figure 3 the mass of the graviton and its p_T spectrum for several number of extra dimensions are shown - the graviton gets "heavier" with increasing number of extra dimension, the p_T spectrum shows almost no dependence on this parameter. Therefore it is not possible to determine the model parameter n from the p_T spectrum, which is similar to the photon spectrum p_T^γ. Figure 4 also indicates that the η distribution of the photon does not offer the possibility to distinguish between the number of extra dimensions. Details of the comparisons at generator level are described in the following.

2.1 Comparisons between SHERPA and PYTHIA for the ADD model

Two generators which provide the Arkani-Hamed, Dvali and Dimoupolos Large extra dimension model have been investigated: PYTHIA and the object-oriented, standalone event generator SHERPA [8] . The generator level studies were therefore performed using the PAX toolkit [9], which provides a standard CMS n-tuple and HepMC interface and allows for fast and efficient generator level comparisons.

The following versions of the generators and analysis tools have been used for the study:

- CMS generator package (CMKIN 4.4.0 [10]) containing PYTHIA 6.2.2.7
- SHERPA 1.06
- PAX toolkit version 2.00.10
- ROOT 5.08.00

The relevant distributions are generated and compared for several benchmark points with $1\ \mathrm{TeV} \leq \mathrm{M_D} \leq 5\ \mathrm{TeV}$ and $2 \leq n \leq 6$. In both generators the CTEQ6L parton distribution set was used. As will be explained later in the

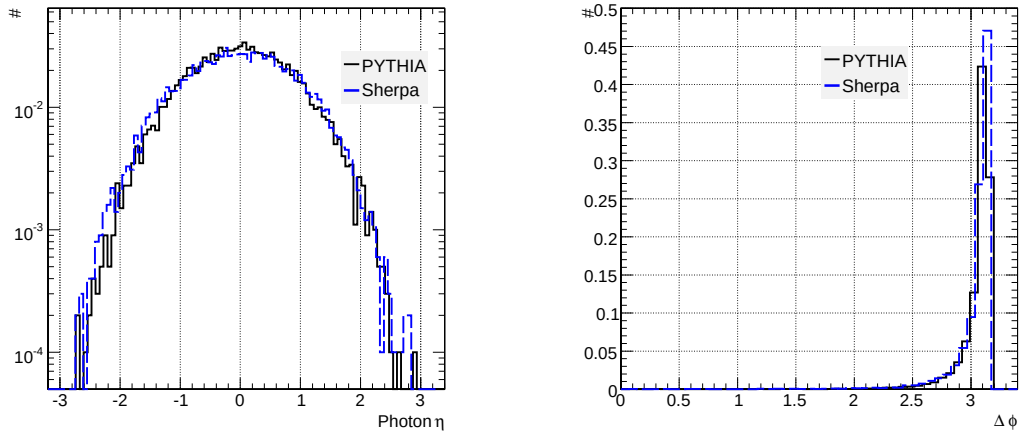

Figure 2: On the left: pseudorapidity of the photon. On the right: angular difference $\Delta\phi$ in the azimuthal plane between the photon and the Graviton (PYTHIA in black, SHERPA in blue(dotted), scenario with two extra dimensions ($n = 2$) and a fundamental scale $\mathrm{M_D} = 5$ TeV).

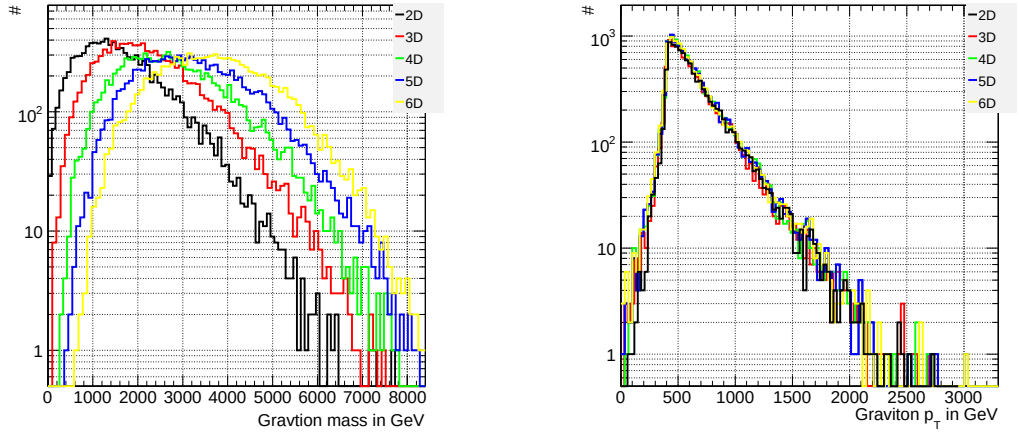

Figure 3: On the left: graviton mass for $\mathrm{M_D} = 5$ and different number of extra dimensions. On the right: graviton p_T; samples generated with PYTHIA.

background section, rough estimates show that the event signature will not be detectable at the LHC in the low-p_T region, because the cross-sections of the backgrounds, particularly of the irreducible $Z^0 + \gamma$ background, is too large. For all signal and background samples therefore a minimum p_T^γ of 400 GeV is consistently requested since the signal cross-section for the theoretically "safer" region ($\mathrm{M_D} > 3.5$ TeV) and the $Z^0 + \gamma$ cross-section are here of the same order.

- PYTHIA 6.2.2.7: $\mathrm{CKIN}(3) > 400$ GeV (CKIN(3) is the minimum partonic center of mass p_T, often named $(\hat{p_\mathrm{T}})$)
- SHERPA 1.06 : $p_T^\gamma > 400$ GeV

In general one can say that the distributions from PYTHIA and SHERPA show good agreement for the benchmark points as is exemplified in the figures. 2, 5 and 6. The cross section tends to be slightly smaller in SHERPA, the differences are on the level of some percent, as can be seen in table 2 and 3 and in figure 7.

M_D	1 TeV	2 TeV	3 TeV	4 TeV	5 TeV
$n = 2$	206.2 fb	12.0 fb	2.5 fb	0.8 fb	0.3 fb
$n = 3$	687 fb	21.0 fb	2.8 fb	0.6 fb	0.22 fb
$n = 4$	2.536 pb	39.0 fb	3.5 fb	0.61 fb	0.16 fb
$n = 5$	10.02 pb	78.0 fb	4.5 fb	0.611 fb	0.128 fb
$n = 6$	44.10 pb	161.0 fb	6.3 fb	0.631 fb	0.10 fb

Table 2: Total cross-sections for the signal for different model parameters calculated by SHERPA with a lower bound on the photon p_T of 400 GeV.

M_D	1 TeV	2 TeV	3 TeV	4 TeV	5 TeV
$n = 2$	221.8 fb	13.8 fb	2.73 fb	0.86 fb	0.35 fb
$n = 3$	753.9 fb	23.5 fb	3.10 fb	0.73 fb	0.24 fb
$n = 4$	2.69 pb	42.0 fb	3.69 fb	0.65 fb	0.17 fb
$n = 5$	10.07 pb	78.6 fb	4.6 fb	0.61 fb	0.12 fb
$n = 6$	39.18 pb	153.0 fb	5.97 fb	0.59 fb	0.10 fb

Table 3: Total cross-sections for the signal for different model parameters calculated by PYTHIA with a lower p_T cut of 400 GeV.

Event Generator	**Cut [GeV]**	**Total cross-section σ [fb]**
CompHEP 4.2p1	$p_T^{Z^0} > 100$	255
Madgraph	$p_T^{Z^0} > 100$	240
SHERPA 1.06	$p_T^{Z^0} > 100$	247
PYTHIA 6.227	$\mathrm{CKIN}(3) > 100$	252
CompHEP 4.2p1	$p_T^{Z^0} > 400$	2.21
Madgraph	$p_T^{Z^0} > 400$	2.28
SHERPA 1.06	$p_T^{Z^0} > 400$	1.9
PYTHIA 6.227	$\mathrm{CKIN}(3) > 400$	2.16

Table 4: Cross-section and settings for different event generator.

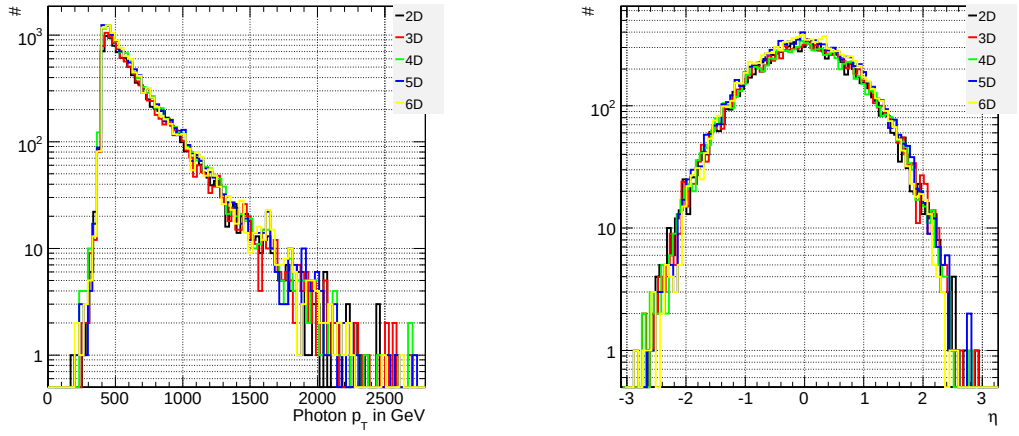

Figure 4: On the left: photon p_T for $\mathrm{M_D} = 5$ and different number of extra dimensions. On the right: the η of the photon; samples generated with PYTHIA.

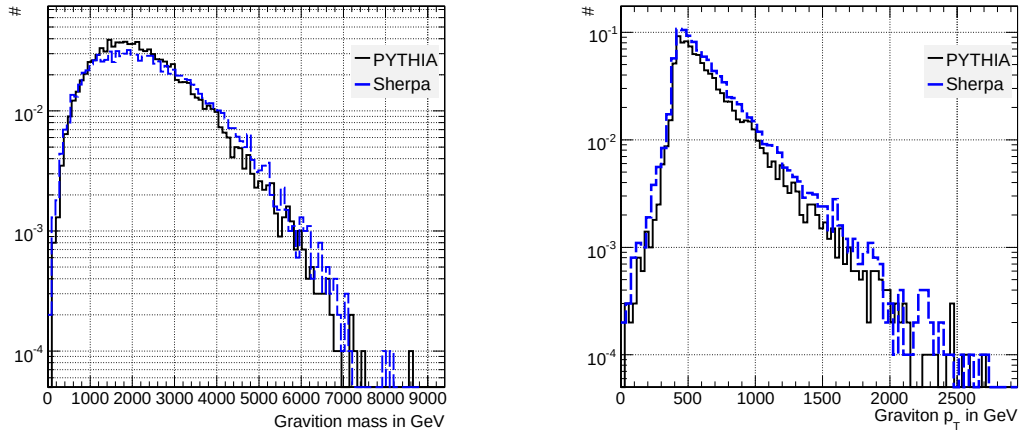

Figure 5: On the left: the mass of the Graviton. On the right: distribution of the graviton transverse momentum p_T^G (PYTHIA in black, SHERPA in blue(dotted), scenario with two extra dimensions ($n = 2$) and a fundamental scale $\mathrm{M_D} = 5$ TeV).

2.2 Event generator comparison for the irreducible background $Z^0 \rightarrow \nu_i \bar{\nu}_i$

In order to estimate the uncertainty on the cross-section and distributions coming from different implementation techniques at generator level, the main irreducible background has been simulated and compared with four different Event generators. (PYTHIA, SHERPA and Comphep and Madgraph) The settings for the process has been chosen as identical as possible. A good agreement between PYTHIA, SHERPA and Comphep has been found up to approximately 1 TeV, where the statistics gets too low. However the cross-section for the high-energetic tail is very low for this background and a relative normalisation to $Z^0 \rightarrow \mu^+\mu^-$ and $Z^0 \rightarrow e^+e^-$ is used to measure this background in the high p_T region.

An overview of the generators and cuts used for this comparison is shown in table 4, the obtained distributions are shown in figure 8. Only Madgraph shows a disagreement, which grows with an increasing production cut; this seems to be a bug and has been reported to the Madgraph team. The other event generators show a good agreement For technical simplicity and consistency, PYTHIA is used in the following to generate this main background (as well as the other backgrounds).

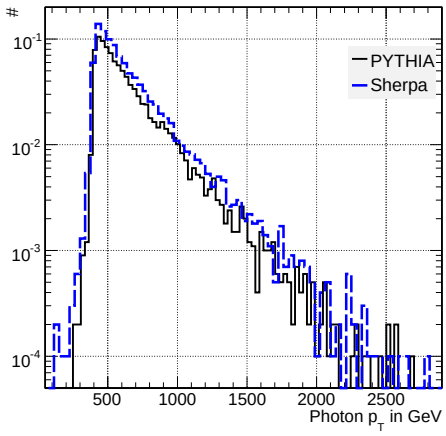

Figure 6: Photon transverse momentum p_T^γ for an effective Planck scale $\mathrm{M_D} = 5000$ GeV and two extra dimensions ($\delta = 2$). (PYTHIA in black, SHERPA in blue(dotted))

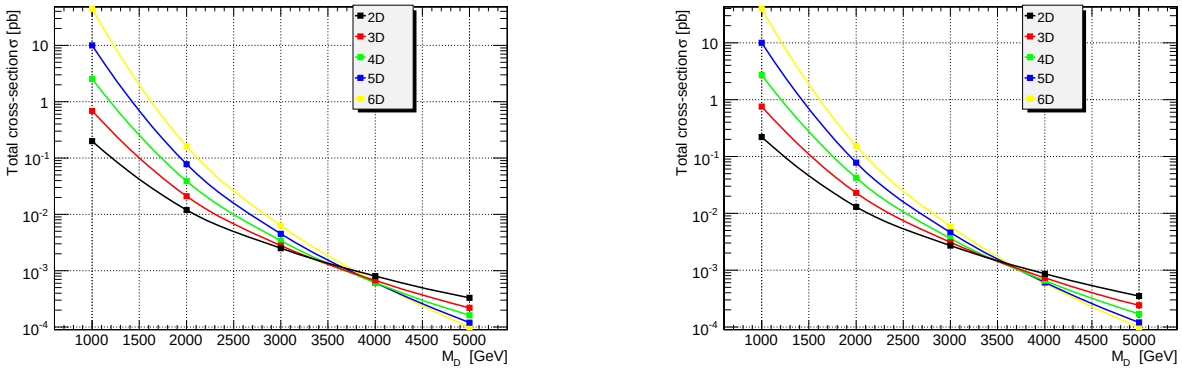

Figure 7: Total cross-section as function of the fundamental scale $\mathrm{M_D} = 5$ for scenarios with different numbers of extra dimensions. (On the left with SHERPA, on the right with PYTHIA)

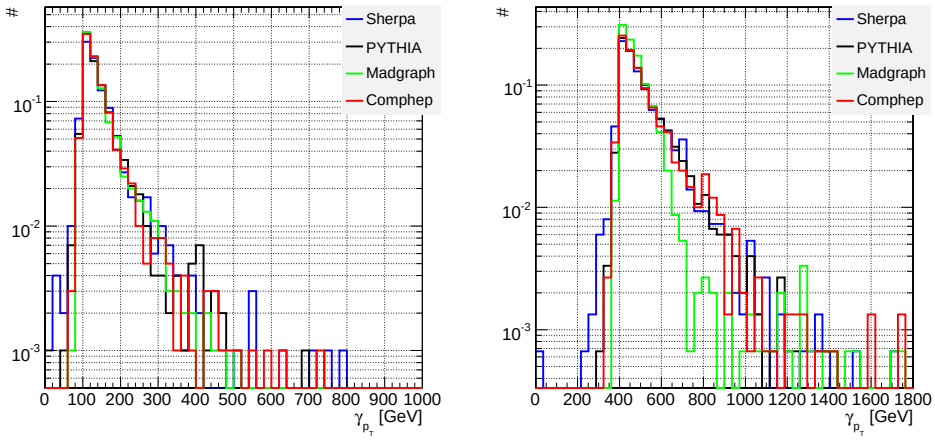

Figure 8: Comparison of the photon p_T for the main background $Z^0 \rightarrow \nu_i \bar{\nu}_i$ with a lower production cut of 100 GeV on the left and 400 GeV on the right for different event generators: Comphep, Madgraph, PYTHIA and SHERPA.

3 Data samples and software

Due to the lack of official full simulated samples, CPU limitations and to increase the statistical precision most samples were produced using the fast simulation [7]. However, small reference samples with the full simulation chain were produced as well in order to compare the relevant physics objects to the fast simulation and to examine the performance of FAMOS for our process.

The following CMS software packages were used to perform the study:

- The generation of proton-proton collisions at 14 TeV center of mass energy is done with CMKIN 4.4.0, based on PYTHIA with the CTEQ6L parton distribution set. The produced samples were used for generator studies, fast and full simulation.
- Most samples were simulated using the CMS fast simulation and reconstruction. All samples include pile-up with diffractive events. The fully simulated samples were produced with OSCAR [5], the Geant4-based CMS simulation package. Geant4 handles the particle propagation and simulates the interactions with the detector in detail. The simulation of the detector response as well as the reconstruction of the fully simulated events was performed with the CMS tool-kit ORCA [6].
- PAX 2.00.10 [9], a CLHEP 2.0 based toolkit for high energy physics is used for the analysis itself.
- ROOT 5.08.00 is for histograms, statistics and fitting.

The data samples produced and used for the analysis are listed below
(all events are generated with a $CKIN(3) > 400$ cut):

- Signal samples: for each $n = 2 - 6, \mathrm{M_D} = 1000 - 5000$ GeV 10,000 fast simulated events,
- 20,000 fully simulated signal events for comparison ($\mathrm{M_D} = 5$ TeV, n = 2).
- 125,000 fast simulated $\gamma + Z^0 \rightarrow \nu_i \bar{\nu}_i$ events
- 60,000 fast simulated QCD events, additional study of this background in different p_{T} bins
- 50,000 fast simulated γ + jets events
- 40,000 fast simulated $W^{\pm} \rightarrow e\nu/\mu\nu$ events
- 40,000 fast simulated $W^{\pm} \rightarrow \tau\nu$ events
- 40,000 fast simulated di-photon events (box and born diagram)
- 10,000 fast simulated $W^{\pm}$+γ events

The following data samples have been produced in addition for the γ+$Z^0 \rightarrow \nu_i \bar{\nu}_i$ "Candle" calibration:

- 20,000,000 generator events with $\gamma + Z^0 \rightarrow \nu\bar{\nu}$ at $CKIN(3) > 50$.
- 20,000,000 generator events with $\gamma + Z^0 \rightarrow \nu\bar{\nu}$ at $CKIN(3) > 300$.
- 135,000,000 generator events $\gamma + Z^0 \rightarrow \mu^+\mu^-$ at various energies.
- 1,000,000 fast simulated $\gamma + Z^0 \rightarrow \mu^+\mu^-$ at $CKIN(3) > 50$.
- 1,000,000 fast simulated $\gamma + Z^0 \rightarrow \mu^+\mu^-$ at $CKIN(3) > 300$.
- 30,000 fully simulated events $\gamma + Z^0 \rightarrow \mu^+\mu^-$ at $CKIN(3) > 50$.
- 30,000 fully simulated events $\gamma + Z^0 \rightarrow \mu^+\mu^-$ at $CKIN(3) > 300$.
- 1,000,000 fast simulated $\gamma + Z^0 \rightarrow e^+e^-$ at $CKIN(3) > 50$.
- 250,000 fast simulated $\gamma + Z^0 \rightarrow e^+e^-$ at $CKIN(3) > 300$.
- 30,000 fully simulated events $\gamma + Z^0 \rightarrow e^+e^-$ at $CKIN(3) > 50$.
- 30,000 fully simulated events $\gamma + Z^0 \rightarrow e^+e^-$ at $CKIN(3) > 300$.

4 Comparisons between CMS full and fast fimulation

Most of the data samples for this study have been produced with the fast simulation FAMOS. Thus, a detailed comparison with respect to the full simulation has been carried out to estimate the accuracy of the fast simulation in our case. The strategy has been as follows: first, the same generated samples were processed with both ORCA and FAMOS and the high-level objects obtained with the CMS analysis package ExRootAnalysis. Then, using the PAX toolkit, the reconstructed quantities can be compared alongside. For this study the following objects of interest are investigated:

- **Photons**: the reconstructed photons has been obtained from the default offline photon candidates. A photon candidate is basically an super-cluster in the electro-magnetic calorimeter(ECAL).
- **Electrons**: the electron candidates are reconstructed and identified with the default configuration of the offline electron reconstruction algorithm. The candidate is essentially an ECAL super-cluster (as in the photon case) with a matched track. In addition, a likelihood for each electron candidate is calculated based on information from the electromagnetic calorimeter and the tracker; A standard package for electron identification which computes the electron likelihood and is available in the ORCA tool-kit. has been used. More details about electron and photon reconstruction in CMS can be found in [2] and [11]. .
- **Muons**: a muon candidate is formed when a muon track is found in the standalone muon system (RPC, CSC, DT) and can be matched to a track in the central silicon tracker.
- **Missing transverse energy**: E_T^{miss} reconstruction is taken as estimate of the missing p_T spectrum from the final state neutrinos. The missing energy is calculated from jets using the iterative cone algorithm with activated muon and electron correction.

4.1 Resolution and efficiency studies

The reconstructed objects are matched to the corresponding generator particles with the objective to compare the resolutions, efficiencies and purities in case of fast and full simulation. The events used for this study are the same that are used later for the normalisation of the main background $\gamma + Z(-> \nu\bar{\nu})$. The electrons used in the comparison are those for which the ElectronLikelihood yields a likelihood of at least 0.65.

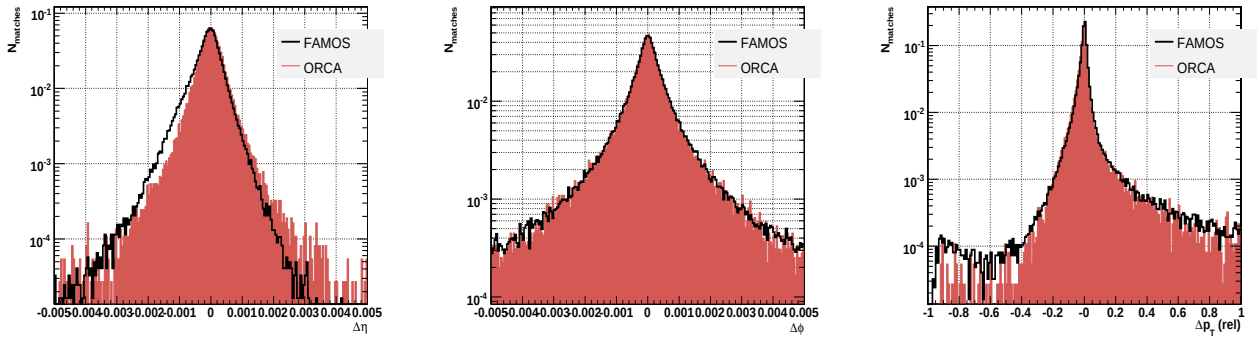

Figure 9: Resolution for electrons in η, ϕ and the relative p_T resolution: the agreement between ORCA and FAMOS is very good and in accordance with the design values [2].

The absolute resolution and the relative resolution are defined as:

$$\Delta X = X_{rec} - X_{gen} \quad (3)$$

$$\Delta X_{(rel)} = \frac{X_{rec} - X_{gen}}{X_{gen}} \quad (4)$$

A combination $\Delta_{combined}$ of the individual resolutions $\Delta\eta$, $\Delta\phi$, $\Delta p_T(rel)$, and their respective standard deviations is used as matching criterion:

$$\Delta_{combined} = \sqrt{(\frac{\Delta\eta}{\sigma_{\Delta\eta}})^2 + (\frac{\Delta\phi}{\sigma_{\Delta\phi}})^2 + (\frac{\Delta p_{T(rel)}}{\sigma_{\Delta p_{T(rel)}}})^2} \quad (5)$$

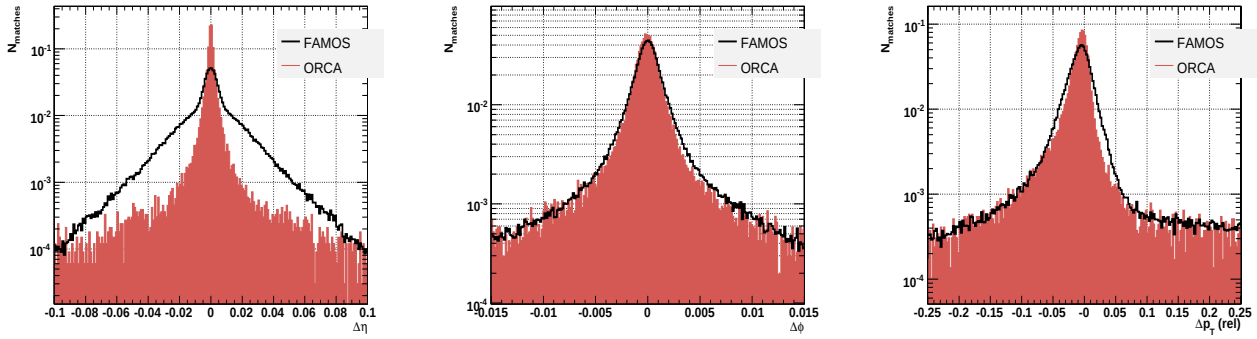

Figure 10: Resolution for photons in η, ϕ and the relative p_T resolution: the agreement between ORCA and FAMOS is very good for p_T and ϕ. The η value is currently not correctly determined in FAMOS and the resolution worse than in ORCA - this will be fixed in the near future.

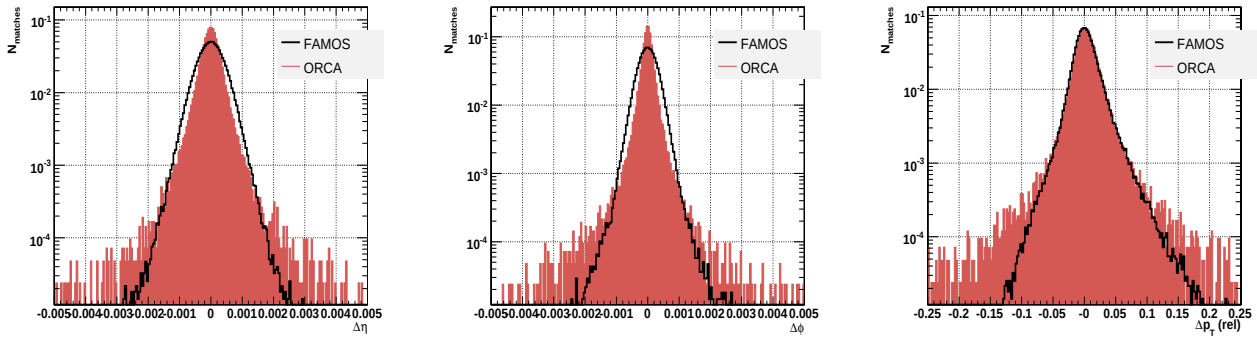

Figure 11: Resolution for muons in η, ϕ and the relative resolution p_T resolution: there is a slight difference between ORCA and FAMOS in η and ϕ, the agreement in p_T is very good.

A pair of a generated and a reconstructed particle is considered as matched when $\Delta_{combined} < 4$. The obtained resolutions for electrons, photons and muons can be seen in figure 9 – 12. In general, the resolutions are consistent with the expected design values and a good agreement between ORCA and FAMOS is found.

When a very high energetic photon hits the center of a crystal, it is possible to have saturation (at about $E_{crystal} > 1.7$ TeV). First studies shows that in this case the energy can be reconstructed up to about 5 % too low. A method to correct the energy using the energy deposition in the surrounding crystals has been recently presented and can be applied for this case [13]. However, in all samples used for this study the probability to have a photon in this p_{T} region is smaller than 1%. The effect from this potential inaccuracy can thus be safely ignored (unless a unexpected large amount will be observed). Another interesting fact noticed during this study was that the Z^0 mass resolution from electrons is better than the resolution obtained using muons for the samples with $CKIN(3) > 400$ GeV.

After having defined a common criterion whether a final state particle has been correctly reconstructed or not, efficiency and purity are compared in dependence of η and p_T.

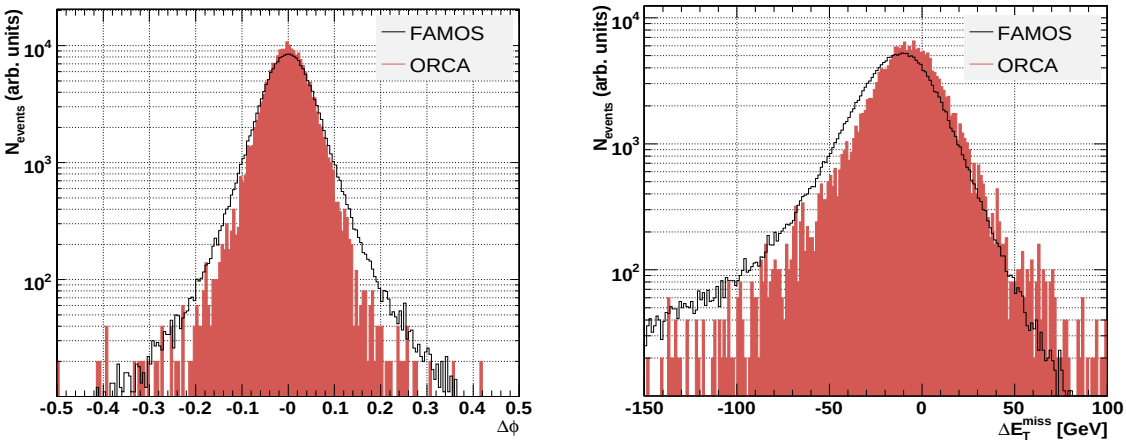

Figure 12: Comparison of the resolution between ORCA and FAMOS for $\not\!\!E_T$ and its ϕ-coordinate.

Reconstructed object		Resolution ORCA	Resolution FAMOS
photon	$\Delta\eta$	$1.5 \cdot 10^{-03}$	$1.7 \cdot 10^{-02}$
	$\Delta\phi$	$1.2 \cdot 10^{-03}$	$1.5 \cdot 10^{-03}$
	$\Delta p_T(rel)$	1.1 %	1.9 %
muon	$\Delta\eta$	$2.7 \cdot 10^{-04}$	$4.1 \cdot 10^{-04}$
	$\Delta\phi$	$1.5 \cdot 10^{-04}$	$4.4 \cdot 10^{-04}$
	$\Delta p_T(rel)$	1.5 %	1.5 %
electron	$\Delta\eta$	$3.5 \cdot 10^{-04}$	$3.8 \cdot 10^{-04}$
	$\Delta\phi$	$5.5 \cdot 10^{-04}$	$5.8 \cdot 10^{-04}$
	$\Delta p_T(rel)$	2.0 %	1.8 %
	ΔE_T^{miss}	17.1 GeV	19.7 GeV
	$\Delta\phi(E_T^{miss})$	$4.2 \cdot 10^{-02}$	$4.9 \cdot 10^{-02}$

Table 5: Overview over resolution ΔX for the relevant objects in this analysis.

In this context, efficiency and purity are defined as:

$$\text{eff} = \frac{\#\text{ matched particles}}{\#\text{generated particles}} \quad (6)$$

$$\text{pur} = \frac{\#\text{ matched partcles}}{\#\text{reconstructed particles}} \quad (7)$$

Again, a good agreement was found for all considered objects, as is exemplified in figure 13 for photons.

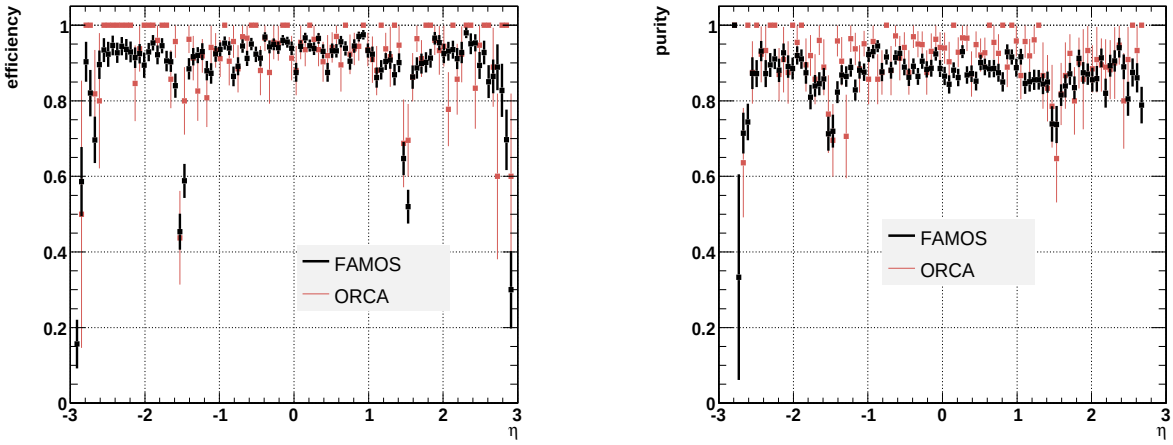

Figure 13: Efficiency and purity for photons as function of η .

This comparison has shown that the performance of FAMOS for efficiency, purity and resolution is quite good and compares with ORCA. Therefore the use of FAMOS in order to increase the statistics and save computing time is justified.

5 The $Z^0\gamma$ "Candle" calibration

In this section a method is described on how the full γ+$Z^0 \rightarrow \nu_i\bar{\nu}_i$ spectrum can be measured from γ+$Z^0 \rightarrow \mu^+\mu^-/e^+e^-$ events. First a conservative set of selection cuts is chosen to be able to reconstruct the "candle" from the final state particles. Then the total acceptance for events which passed the candle selection is studied as well as the estimate of the reconstruction efficiencies.

5.1 γ+$Z^0 \longrightarrow \mu^+\mu^-/e^+e^-$ selection

In order to reconstruct the lepton pair reliably with good precision, some kinematic and topological constraints are imposed. For the selection of γ+$Z^0 \longrightarrow \mu^+\mu^-$ events the following selection criteria on the reconstructed final state particles are applied:

- The single hard photon has to be found in a pseudo-rapidity range of $|\eta_\gamma| < 2.7$ in the ECAL. In the high-p_T range of interest ($p_T^\gamma > 400$ GeV) practically all photons in γ+Z^0 signals will be in that range.
- The selection criteria of the muons are chosen as follows:
  - Both muons from the Z^0 decay are required to have a minimum transverse momentum $p_T^{\mu^\pm} > 20$ GeV to be reliably found by the muon trigger (the single muon trigger uses a nominal cut of 14 GeV for the L1 trigger and 19 GeV for the HLT).
  - In order to avoid effects on the edge of the muon system, both muons are required to be within $\eta_{\mu^\pm} < 2.3$. The muon reconstruction efficiency would quickly drop at the edges of the muon system coverage and impose unwanted uncertainties on the reconstruction efficiency otherwise.

Similarly the following criteria are applied for the selection of γ+$Z^0 \longrightarrow e^+e^-$ events:

- The electrons are identified using a likelihood approach (standard electron likelihood module included in the ORCA reconstruction package) with a discriminator cut at 0.65.
- The electrons are required to have a minimum transverse momentum $p_T^{e^\pm} > 20$ GeV like the muons.
- For the electron identification it is important to find the electron track, so the η limit is imposed by the tracking system and electrons are only accepted with $\eta_{e^\pm} < 2.4$.

For both kind of events the common selection criteria on the photon and the reconstructed Z^0 are:

- The reconstructed Z^0 is required to be found within the mass window of $80\ \mathrm{GeV} < \mathrm{m_{Z^0}} < 100\ \mathrm{GeV}$.
- The γ and Z^0 are required to be back-to-back in the $x-y$ plane, $\Delta\phi(\gamma, Z^0) > 2.5$
- Both particles form the decay of the Z are required to be within 50% of their average p_T as follows: $|\frac{p_T^\gamma - p_T^{Z^0}}{p_T^\gamma + p_T^{Z^0}}| < 0.25$

5.2 γ+$Z^0 \longrightarrow \mu^+\mu^-/e^+e^-$ acceptance

In the following, the reconstruction efficiency and the detector acceptance are studied separately. The reconstruction efficiency can be approximated via simple p_T dependent functions. The detector acceptance is highly dependent on the topology of the event.

To reliably normalise the γ+$Z^0 \rightarrow \nu_i\bar{\nu}_i$ predictions using the γ+$Z^0 \rightarrow \mu^+\mu^-$ data, the detector acceptance is parameterised as a function of the p_T and η of the photon. The acceptance α for high-p_T events ($p_T^\gamma > 400$ GeV) after the subsequent selection cuts is shown in figure 14.

The total acceptance as a function of η is not constant for different p_T^γ regions. It is rather different in the low-p_T range ($p_T^\gamma \approx 100$ GeV) where the pseudo-rapidity distribution of the Z^0 is similar to the distribution of a single Z^0 production.

The detector acceptance is parameterised using a two-dimensional function $\alpha(p_T^\gamma, \eta_\gamma)$. The inverse of this function is used as a weighting function for accepted events to transform the measured photon p_T distribution to the full p_T^γ spectrum. With this method, the p_T^γ spectrum of γ+$Z^0 \rightarrow \nu_i\bar{\nu}_i$ can be normalised to the one weighted for acceptance and efficiency from the candle sample.

The acceptance function $\alpha(p_T^\gamma, \eta_\gamma)$ is obtained by fitting even tchebycheff polynomials of sixth order (four parameters) in different p_T^γ slices in the range between $100\ \mathrm{GeV} < \mathrm{p_T^\gamma} < 1200$ GeV and then describing the chebycheff coefficients in turn by fifth-order polynomials. The overall fit χ^2/ndf is close to 1.

The acceptance for the electron based calibration is done in an identical way and only differs by the slightly larger electron η cut. The average acceptance numbers resulting from the study are shown in table 6.

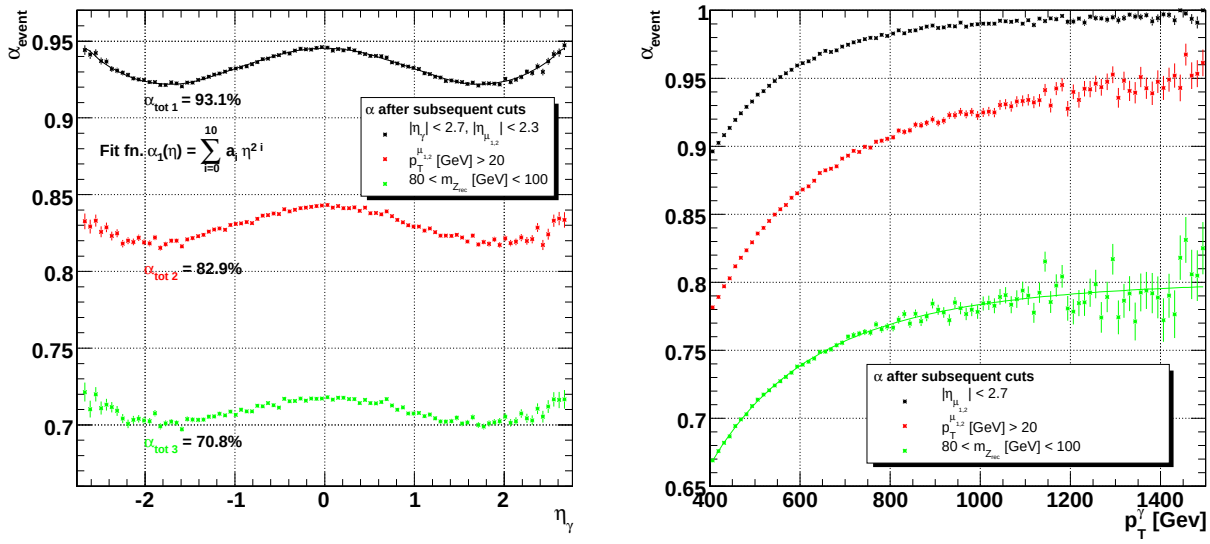

Figure 14: Acceptance α for high-p_T events ($p_T^\gamma > 400$ GeV) after using all candle selection criteria.

γ+$Z^0 \to \mu^+\mu^-$		γ+$Z^0 \to e^+e^-$	
cut	**acceptance**	**cut**	**acceptance**
$\lvert\eta_\gamma\rvert < 2.7, \lvert\eta_{\mu^\pm}\rvert < 2.3$	93.1%	$\lvert\eta_\gamma\rvert < 2.7, \lvert\eta_{e^\pm}\rvert < 2.4$	94.6%
$p_T^{\mu^\pm} > 20$ GeV	82.9%	$p_T^{e^\pm} > 20$ GeV	84.1%
80 GeV $< m_{Z^0} <$ 100 GeV	70.8%	80 GeV $< m_{Z^0} <$ 100 GeV	71.8%

Table 6: Remaining γ+$Z^0 \to \mu^+\mu^-/e^+e^-$ after each cut for $p_T^\gamma > 400$ GeV

5.3 γ+$Z^0 \to \mu^+\mu^-/e^+e^-$ reconstruction efficiency

The transformation method based on the generator study using $\alpha(p_T^\gamma, \eta_\gamma)$ is now tested against the detector simulation fin order to parameterise the reconstruction efficiency effects. Due to limitations in CPU time, the simulation has been mostly done with the fast simulation FAMOS at high statistics.

After the transformation, the number of events in the different p_T^γ and η_γ bins is compared to the number of expected events in these bins assuming an ideal detector with full 4π coverage (i.e. the generator information). The reconstruction efficiency thus obtained with FAMOS is shown in figure 15. Again the results for the electrons are very similar and not shown explicitly.

The reconstruction efficiency is composed of several factors. One photon and two muons have to be reconstructed. Furthermore, the reconstructed Z^0 has to pass the mass window constraint. The reconstruction of its invariant mass requires an accurate measurement of the muon kinematics. The main limiting factor here is the momentum measurement, especially for muons with high p_T values since their tracks become rather straight and a precise momentum measurement is challenging. This leads to a smearing of the Z^0 mass peak and deteriorate the efficiency in the high-p_T range.

The reconstruction efficiencies are mostly flat as function of η_γ except for the ECAL gap between barrel and endcap (at about $\eta = 1.5$). As long as there is no interest in precise measurement of the η distributions the efficiency can be assumed to be constant in η_γ for a given p_T^γ and is slightly falling for larger p_T^γ values. A very simple approximation is done here via a linear fit through the data points of the FAMOS simulated efficiency:

$$\epsilon_{rec}(p_T^\gamma) = \epsilon_{rec}^0 + \epsilon_{rec}^1 \cdot p_T^\gamma \tag{8}$$

The total reconstruction efficiency ϵ_{tot} can be expressed as

$$\epsilon_{tot} = \alpha(p_T^\gamma, \eta_\gamma) \cdot \epsilon_{rec}(p_T^\gamma) \tag{9}$$

In table 7, the detector acceptance and the reconstruction efficiencies using the fast (FAMOS) and the full detector

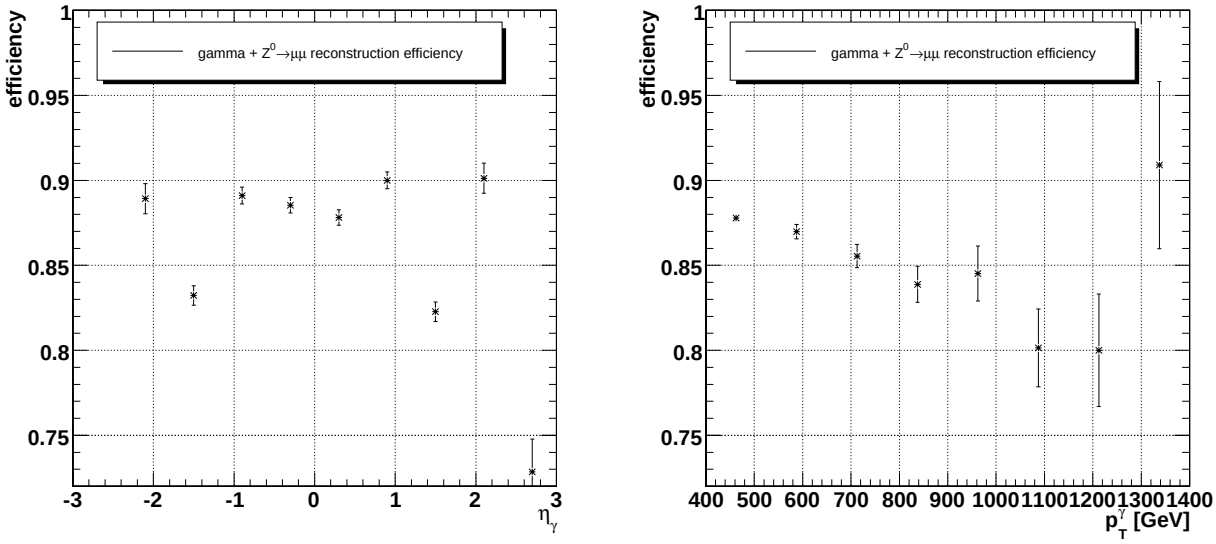

Figure 15: Reconstruction efficiency ϵ_{rec} for high-p_T events ($p_T^\gamma > 400$ GeV) passing all selection criteria as function of p_T^γ and η^γ .

simulation (ORCA) are listed.

Cut	Sample	Detector acceptance	Reconstruction efficiency		Total efficiency	
			FAMOS	ORCA	FAMOS	ORCA
$p_T^\gamma > 100$ GeV	γ+$Z^0 \to \mu^+\mu^-$	39.2%	94%	93%	37%	36%
	γ+$Z^0 \to e^+e^-$	45.3%	90%	89%	41%	40%
$p_T^\gamma > 400$ GeV	γ+$Z^0 \to \mu^+\mu^-$	70.8%	87%	83%	62%	59%
	γ+$Z^0 \to e^+e^-$	71.8%	82%	83%	59%	60%

Table 7: Detector acceptance, reconstruction efficiencies and the total efficiency using the fast (FAMOS) and the full detector simulation (ORCA).

As can be seen in table 7, FAMOS and ORCA slightly differ in the reconstruction efficiency. The uncertainty is of the same order of magnitude as the statistical uncertainty from the total number of observable events ($< 3\%$ after $30 fb^{-1}$ of γ+$Z^0 \to \mu^+\mu^-/e^+e^-$).

5.4 Kinematics and E_T^{miss} in γ+$Z^0 \to \mu^+\mu^-/e^+e^-$ and γ+$Z^0 \to \nu_i\bar{\nu}_i$

To prove that the normalisation method using the measured γ+$Z^0 \to \mu^+\mu^-$ events corrected for acceptance $\times$ efficiency (Eq. 9) can be used to calibrate the γ+$Z^0 \to \nu_i\bar{\nu}_i^-$ events, the p_T distributions for the γ and the Z^0 (reconstructed from the muons for $Z^0 \to \mu^+\mu^-$ and E_T^{miss} in the $Z^0 \to \nu_i\bar{\nu}_i$ case) are compared.

Figure 16 shows the measured and the derived p_T^γ spectrum from γ+$Z^0 \to \mu^+\mu^-$ in comparison with the generator spectrum for γ+$Z^0 \to \nu_i\bar{\nu}_i$ events. Since the p_{T} spectrum of the Z^0 at generator level corresponds to the photon p_T^γ spectrum, the weighted γ+$Z^0 \to \mu^+\mu^-$ spectrum delivers a precise approximation of both true spectra.

The particle balancing the transverse momentum of the photon in γ+Z^0 events is the Z^0. While the Z^0 can be reconstructed from the leptons ($\mu^+\mu^-$ and e^+e^- respectively) it shows up as missing transverse energy (E_T^{miss}) when the Z^0 decays into neutrinos. The $E_T^{Z^0}$ spectrum from the derived γ+$Z^0 \to \mu^+\mu^-$ events compared with the reconstructed E_T^{miss} in the γ+$Z^0 \to \nu_i\bar{\nu}_i$ case can be seen in figure 17. The distributions are not expected to be identical. One of the reasons for the difference is that the E_T^{miss} reconstruction in CMS is not very accurate compared to the precise reconstruction of the Z^0 from muons or electrons. The derived spectrum gives a better description of the true $Z^0 \to \nu_i\bar{\nu}_i$ distribution.

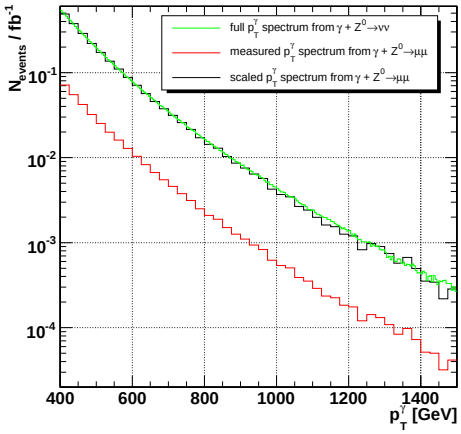

Figure 16: Number of expected p_T^γ events per 25 GeV bin at 1fb^{-1} from measured γ+$Z^0 \to \mu^+\mu^-$ events before and after transformation compared with the generator distribution for γ+$Z^0 \to \nu_i\bar{\nu}_i$. The transformed muon distribution models the $\nu_i\bar{\nu}_i$ spectrum well.

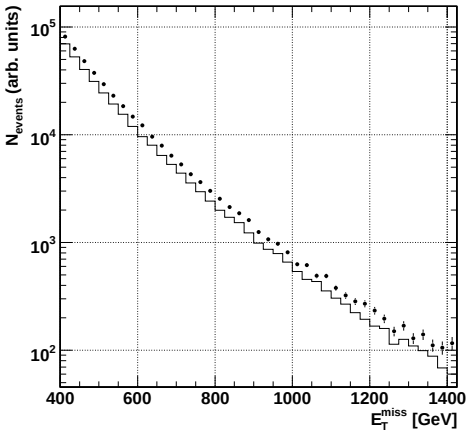

Figure 17: E_T^{miss} distribution comparison between γ+$Z^0 \to \nu_i\bar{\nu}_i$ and transformed γ+$Z^0 \to \mu^+\mu^-$ events ($E_T^{Z^0}$ used as E_T^{miss}).

The average multiplicative factors going into the derivation are shown in table 8.

Cut	γ+$Z^0 \to \mu^+\mu^-$			γ+$Z^0 \to e^+e^-$		
	$1/\epsilon_{tot}$	$\frac{br_{Z^0\to\nu_i\bar{\nu}_i}}{br_{Z^0\to\mu^+\mu^-}}$	**total**	$1/\epsilon_{tot}$	$\frac{br_{Z^0\to\nu_i\bar{\nu}_i}}{br_{Z^0\to e^+e^-}}$	**total**
$p_T^\gamma > 100$ GeV	2.71	5.96	16.2	2.45	5.96	14.6
$p_T^\gamma > 400$ GeV	1.62		9.68	1.70		10.2

Table 8: transformation factors for γ+$Z^0 \to \nu_i\bar{\nu}_i$ calibration

5.5 Statistical and systematical limitations at high p_T

The total number of expected events from γ+$Z^0 \to \mu^+\mu^-$ and γ+$Z^0 \to e^+e^-$ in the high- and low-p_T range ($p_T > 400$ GeV and $p_T > 100$ GeV respectively) as well as the number of γ+$Z^0 \to \nu_i\bar{\nu}_i$ events that are used for the calibration are shown in table 9.

Due to the very small cross-section in the high-p_T range above 400 GeV the whole study has been extended down to the much lower $p_T > 100$ GeV cut to get more statistics. Doing this, however, raises the problem of how the distribution obtained can be extrapolated into the high-p_T range. If the Monte Carlo prediction for the shape of the p_T^γ distribution can be trusted it can be compared to the measured shape of the spectrum. Note that no k-factors

which might increase the expected statistics of the candle sample are taken into account.

Events		$p_T^\gamma > 100$ GeV			$p_T^\gamma > 400$ GeV		
sample	**int. luminosity**	**all**	**observable**	**stat. error**	**all**	**observable**	**stat. error**
γ+$Z^0 \to \mu^+\mu^-$	$10 fb^{-1}$	485	177	7.5%	3.8	2.2	67%
	$30 fb^{-1}$	1460	530	4.3%	11.4	6.7	38%
γ+$Z^0 \to e^+e^-$	$10 fb^{-1}$	485	196	7.1%	3.8	2.6	61%
	$30 fb^{-1}$	1460	590	4.1%	11.4	8.0	35%
combined	$10 fb^{-1}$	970	390	5.1%	7.6	5.3	45%
	$30 fb^{-1}$	2910	**1170**	**2.9%**	23	16	26%
γ+$Z^0 \to \nu_i\bar{\nu}_i$	$10 fb^{-1}$				23	21	22%
	$30 fb^{-1}$				69	**62**	**13%**

Table 9: Number of events (efficiency estimations from OSCAR/ORCA) and resulting statistical uncertainty

The acceptance correction function has been obtained using the leading order event generator PYTHIA. This contributes an unknown systematics uncertainty from the Monte Carlo calculations that cannot be corrected away by the calibration. The acceptance correction relies on the correct prediction of the angle distribution between the Z^0 and the photon at different energies. Since both particles are not charged the error is estimated to be small but next to leading order (NLO) calculations would improve the situation.

6 Trigger path

The topology of signal events is simple. The main trigger path will be the single photon trigger, both at the fast Level 1 trigger(L1) and the High Level Trigger(HLT). Presently the single photon trigger has a HLT level threshold of 80 GeV, which is far below the selection cut for events with isolated photons above 400 GeV. Hence the expected trigger efficiency is close to 100%. The efficiency can be monitored from data with a $\not\!\!E_T$ trigger, which will have a threshold in the range of 200-300 GeV, well below the acceptance of the bulk of the signal data.

7 Analysis of the CMS sensitivity for Large Extra Dimensions

All signal and background samples used in the following analysis were simulated using the fast detector simulation FAMOS. The backgrounds considered in this analysis and their total cross-sections are listed in table 10 and discussed below:

- The largest irreducible background is the di-boson production of $\gamma + Z^0 \to \nu_i\bar{\nu}_i$; the invisible decay of the Z^0 gives rise to a large $\not\!\!E_T$ rendering this process signal-like. This major background has been studied in detail and discussed separately in the previous section, where a normalisation method of this background from measured data is presented.
- The di-boson production γ+$W\pm \to e\nu$ is another background, when the electron is lost or fakes a photon.
- A contribution is expected as well from the direct W production. The W boson decays in 10.72% into $W\pm \to e\nu$; the neutrinos show up in the detector as $\not\!\!E_T$. The electrons can be misidentified as photon. This background, as well as all backgrounds containing highly-energetic charged particles (e, μ, jets, etc...) can be suppressed using a high-p_T track veto.
- γ+$W\pm \to \mu\nu$ where the muon is lost and a bremsstrahlung photon is produced.
- $W\pm \to \tau(\to e\nu\bar{\nu})\nu$ is considered as well.
- QCD production can contribute to the background if a jet fakes a photon or is grossly miss-measured, so a dijet event can look like a γ+$\not\!\!E_T$ event.

- γ+ jets events will appear as $\gamma + \not\!\!E_T$ events, if the jet is not measured correctly or lost (i.e. along the beam pipe).
- $Z^0 \rightarrow \nu\bar{\nu}$+ jets is also a potential background, since it always has a natural amount of $\not\!\!E_T$; It can only be suppressed by a photon reconstruction with high purity and an efficient rejection of jets faking photons or non isolated photons in jets.
- Di-γ events (box and born diagram) where one γ is lost.
- Cosmics have been the largest background at CDF in a similar analysis. The CDF detector is however situated closer to the surface. A muon may give rise to $\not\!\!E_T$ and/or create a bremsstrahlung photon. The same problem can occur with muons originating from the beam halo. However such events must coincide with an LHC event registered by the trigger. The study of this background class requires full detector simulation to correctly handle the time stamp information of the event, to which the cosmic or beam halo muon would contribute. The possible impact of these effects for this analysis at the CMS detector has not yet been investigated. It is planned to perform this study as next step - so far only a rough estimate on the rate can be given.

Background	σ **for** $\hat{p_T} > 400$ GeV
$Z^0\gamma \rightarrow \nu\bar{\nu} + \gamma$	2.16 fb
$W^{\pm} \rightarrow e\nu$	18.2 fb
$W^{\pm} \rightarrow \mu\nu$	18.2 fb
$W^{\pm} \rightarrow \tau\nu$	18.2 fb
$W^{\pm}\gamma \rightarrow e\nu$+$\gamma$	0.83 fb
γ+Jets	2.50 pb
QCD	2.15 nb
di-γ born	5.20 fb
di-γ box	0.14 fb
Z^0 + jets	0.69 pb

Table 10: Total cross-sections for the Standard Model backgrounds considered in this study.

Background	**Rate for** $p_T^{\mu} > 400$ GeV
Cosmic muons	11 Hz
Beam Halo	1 Hz

Table 11: Estimated rates for cosmic and beam halo muons (from CMKIN cosmic muon generator and first beam-halo studies.)

7.1 Analysis path and cut efficiency on signal and backgrounds

Besides of the kinematic cut on the partonic centre of mass p_T ($\widehat{p_T}$) at generator level, only photons with a transverse momentum larger than 15 GeV have been considered in this analysis, since only very high-energetic photons are relevant for this study. With a simple set of cuts already a notable suppression of the backgrounds is possible. Depending on the model parameters a more or less significant excess of $\gamma + \not\!\!E_T$ events can be observed. The following analysis cuts have been chosen:

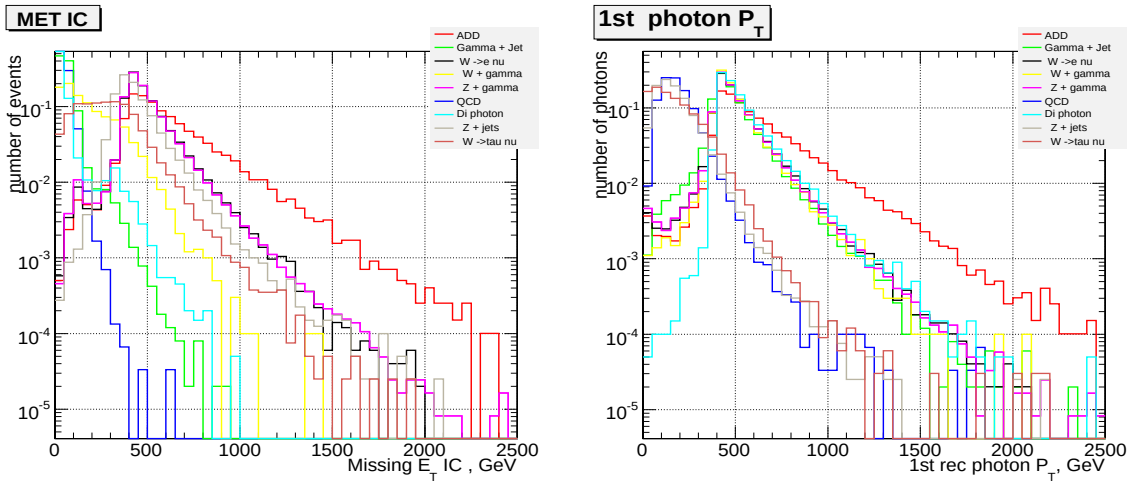

Figure 18: Normalised distributions for signal and background for $\not\!\!E_T$ (left) and p_T^γ (right).

1. At least $\not\!\!E_T > 400\,\mathrm{GeV}$ is requested. This cut significantly reduces the QCD, the γ+jets and di-photon background where no high $\not\!\!E_T$ is expected. The normalised $\not\!\!E_T$ distributions for signal (as an example signal a scenario with $\mathrm{M_D} = 5\,\mathrm{TeV}$, $n = 2$ is chosen for the following plots) and background can be seen in figure 18.

2. The photon p_T has to be above $400\,\mathrm{GeV}$, too. This reduces the background with softer photons as can be seen in figure 18.

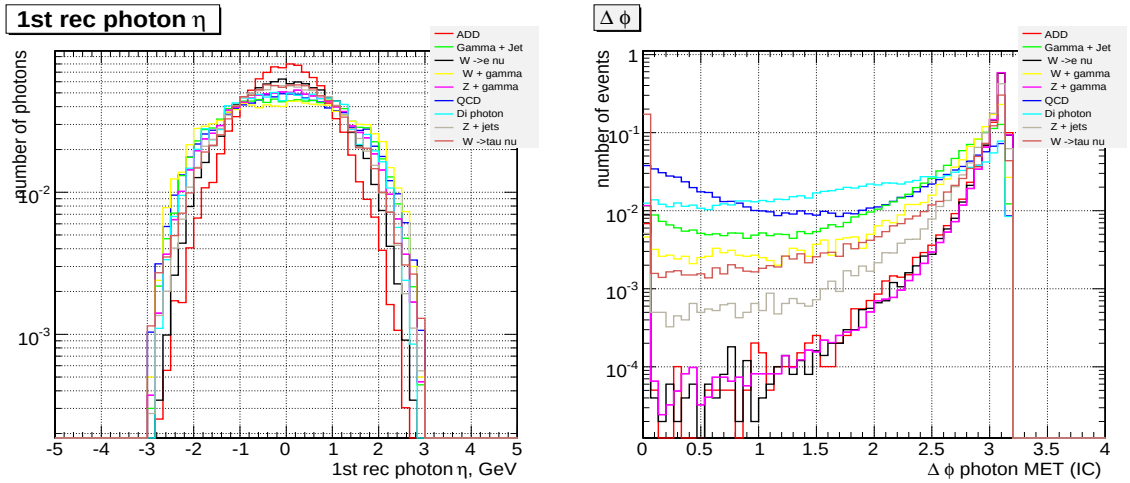

Figure 19: Normalised distributions for signal and background showing the pseudorapidity of the photon, η^γ, (left) and the difference $\Delta\phi$ between the photon and $\not\!\!E_T$(right).

3. The final state photon and graviton are back-to-back -therefore a cut on the difference in ϕ can be applied to reduce background which do not have this characteristic, see figure 19. We demand a $\Delta\phi(\not\!\!E_T, \gamma) > 2.5$.

4. Since the signal photons are produced in the central detector region (figure 19), a $\|\eta\| \leq 2.4$ is required.

5. A track veto for high p_T tracks > 40 GeV is applied. This is a powerful criterion to reduce all background containing high-energetic charged particles (e, μ, jets) (see figure 20.)

6. During the analysis a contamination with fake photons originating from jets has been detected, which results in a non negligible background contribution due to the high cross-section. Therefore, an Isolated Photon Likelihood L has been applied as well.

To reduce the backgrounds containing jets an *H/E* cut or a cut on the number of jets have been also studied. *H/E* is the ratio of the energy deposited in the hadronic calorimeter divided by the energy deposited in the electromagnetic calorimeter. This criterion is well suited to distinguish photons from jets, which have naturally higher *H/E* values. However, this cut significantly only reduces the QCD and γ+jets background, which are already highly suppressed. It does not suppress significantly the Z^0 + jets background. Therefore an *Isolated Photon Likelihood* has been

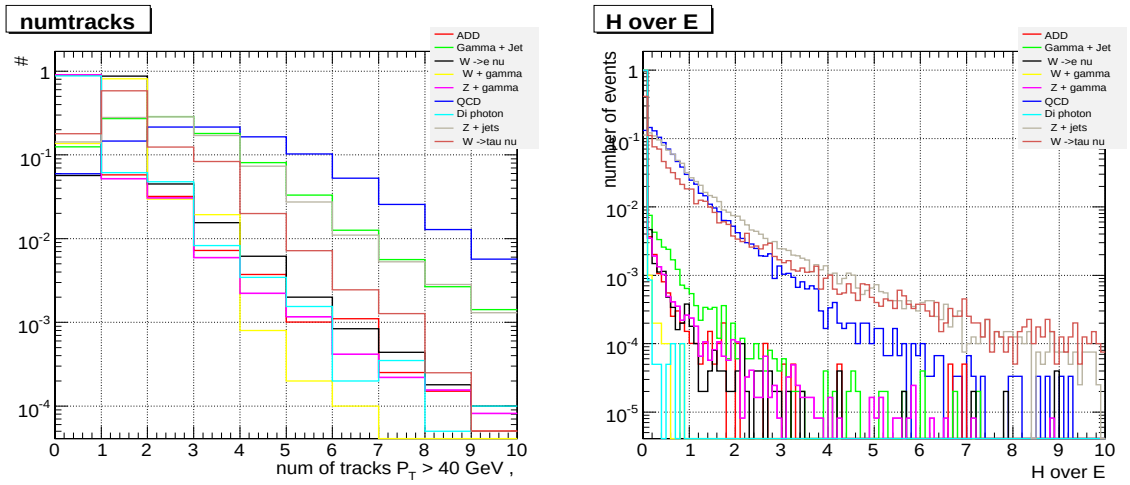

Figure 20: Normalised distributions for signal and background showing the number of tracks with a $p_{\mathrm{T}} > 40$ GeV (left) and *H/E* for the most energetic super-cluster (right.)

introduced to reject jets faking photons or non-isolated photons. It was designed following the example of the Electron Likelihood in ORCA and calculates the Likelihood from a set of reference histograms for signal and background. It uses the following input variables:

- $\frac{EMax}{E3x3}$, i.e. the ratio of the energy deposition in the highest-energetic ECAL crystal relative to the 3x3 matrix as shower shape variable to suppress pions.
- $\frac{E3x3}{E5x5}$ to also take the energy deposition in the 3x3 matrix with respect to the 5x5 matrix into account.
- The total momentum of all tracks around the photon in a $\Delta R < 0.3$ cone with $\Delta R = \sqrt{(\Delta\eta)^2 + (\Delta\phi)^2}$.
- The relative amount of energy in the hadronic calorimeter(HCAL) in all clusters around the photon in a $\Delta R < 0.3$ cone compared to the energy deposited in the ECAL.
- The distance to the nearest track.

With this approach the misidentification of jets as photons can be completely suppressed. In a small fraction of Z^0+$jets$ events one of the quarks can radiate an isolated high-energetic photon while the jet is very soft and not reconstructed, which makes the event look like a signal candidate and irreducible. This topology is very unlikely, but due to the high total cross-section of the Z^0+ jets prodcution it still delivers a non negligible contribution. The Candle calibration method from data presented in the last section will take this type of events intrinsically into account. For all data samples the signal acceptance and background rejection have been evaluated. Signal samples corresponding to ADD scenarios with 2, 3, 4, 5 and 6 extra dimensions have been investigated - as for the second model parameter, the fundamental scale $\mathrm{M_D}$, it turns out that $\mathrm{M_D}$ is only a scale factor and does not distort the distributions - therefore, for different $\mathrm{M_D}$'s only the total number of expected events has been scaled, since the selection efficiency remains constant. The calculation of the number of expected ADD events is challenging from the theoretical point of view: there are no further constraints on the value of $\mathrm{M_D}$ except for the lower bounds which has been established by LEP. However, going to low $\mathrm{M_D}$ values imposes the following problem: a fraction of the events has a partonic center of mass energy above the effective Planck scale, which leads to transplanckian graviton production. The ADD model is valid only below $\mathrm{M_D}$ which is the scale where gravity becomes strong and only a (not available) theory of quantum gravity or string theory would be able to make predictions in this region. Therefore, the ADD cross-sections are rescaled by an acceptance factor α, which only chooses events with a graviton mass below the effective Planck scale, $\mathrm{M_D} > \mathrm{m_G}$. The (rescaled) cross-sections of the ADD signal and its major backgrounds, the cut performance and the number of expected events for $30\ \mathrm{fb}^{-1}$ and $60\ \mathrm{fb}^{-1}$ are summarised in table 12.

A detailed study of the expected signal events for a set of sample points in the $\mathrm{M_D}, n$ parameter space has been performed using Pythia. In table 13 the total cross-sections of the ADD Graviton + Photon production are listed. As described above, the cross-section are truncated and events with $\mathrm{M_D} < m_G$ are rejected, since they have been produced in the trans-Planckian region. The acceptance naturally gets smaller at lower values of $\mathrm{M_D}$. Since the Graviton gets heavier with increasing number of extra dimensions the acceptance also gets lower with increasing n - this can be seen in table 14. The influence of this hard truncation method is shown in table 15, where the

Sample	$\not{E}_T >$ 400 GeV	$p_T^\gamma >$ > 400 GeV	$\|\eta_\gamma\|$ < 2.4	$\Delta\Phi$ > 2.5	**track veto** > 40 GeV	$L >$ 0.2	**Events for** 30 fb^{-1}
ADD	88.60%	85.52%	85.52%	84.67%	77.40%	75.10%	8.1
γ+Z^0	81.29%	75.66%	74.61%	74.11%	68.44%	67.42%	43.7
γ+$W^\pm$	8.59%	8.42%	8.39%	8.35%	3.35%	3.32%	0.8
QCD	0.01%	0.01%	0.01%	0.01%	0.00%	0.00%	< 3
di-γ born	1.19%	1.16%	1.16%	1.12%	1.00%	0.98 %	1.5
di-γ box	0.75%	0.61%	0.61%	0.44%	0.34%	0.34%	0.01
$W^\pm \to e\nu$	82.27%	76.05%	75.75%	75.11%	3.96%	3.50%	19.1
$W^\pm \to e\mu$	88.34%	0.20%	0.19%	0.09%	0.00%	0.00%	< 3
$W^\pm \to e\tau$	21.15%	4.21%	4.20%	4.11%	0.92%	0.40%	2.2
γ+jets	0.31%	0.05%	0.05%	0.03%	0.01%	0.00%	< 3
Z^0+jets	52.86%	2.78%	2.76%	2.59%	0.29%	0.04%	8.2

Table 12: Signal ($\mathrm{M_D} = 5$ TeV, $n = 2$) and background efficiency for the applied cuts and number of expected events for an integrated luminosity of 30 fb^{-1}.

.

effective cross sections are listed. In the next table 16 the cut efficiency ϵ - i.e. the percentage of signal events surviving all applied cuts - is shown. With this strategy one can calculate the number of expected events as $N_{exp} = \sigma_{\mathrm{tot}} * \alpha(\mathrm{m_G}) * \epsilon$.

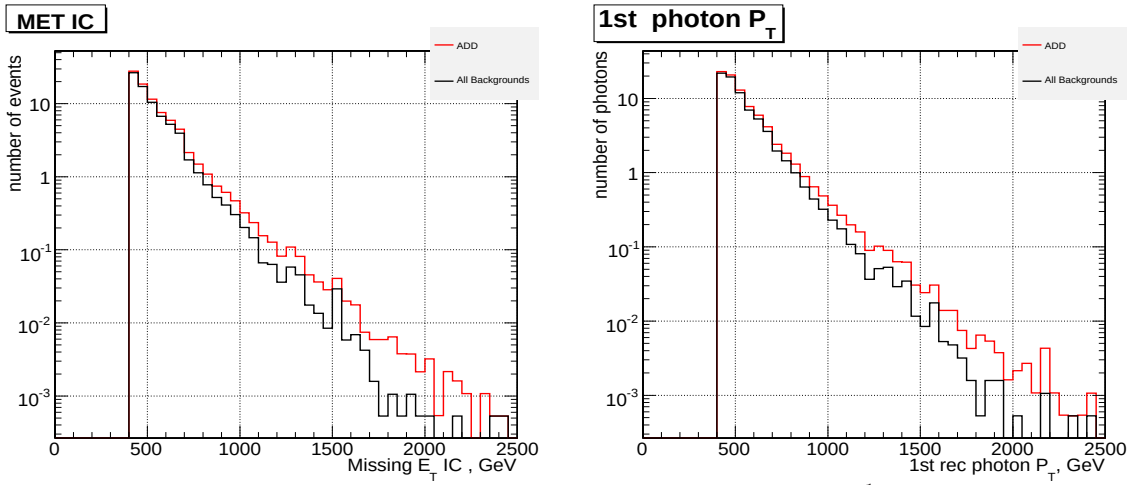

Figure 21: Signal and all backgrounds for $\not{E}_T$ after all cuts normalised to 60 fb^{-1} for $\mathrm{M_D} = 5$ TeV, $n = 2$ ($\not{E}_T$ left, reconstructed photon p_T right).

The signal would show up as an excess over the expected number of Standard Model background events - this is exemplified in figure 21 and figure 22 , where the photon spectrum and the $\not{E}_T$ spectrum are shown in the case of a discovery of a $\mathrm{M_D} = 5$ TeV, $n = 2$ and $\mathrm{M_D} = 2.5$ TeV, $n = 2$ scenario. In table 18 the significance $\mathrm{Sig} = 2(\sqrt{\mathrm{S+B}} - \sqrt{\mathrm{B}})$ is calculated for each ADD scenario. It can be seen that up to $\mathrm{M_D} = 3$ a $5\,\sigma$ discovery for all n is possible. It should be noted that due to the hard truncation this is a conservative approach and should be considered as lower bound for the expected significances. A less conservative approach is to reduce the cross-section by a damping factor. This has been applied for example by ATLAS [14] using the damping factor $M_D^4/\hat{s}^2$ when $\hat{s}^2 > M_D^2$(soft truncation).

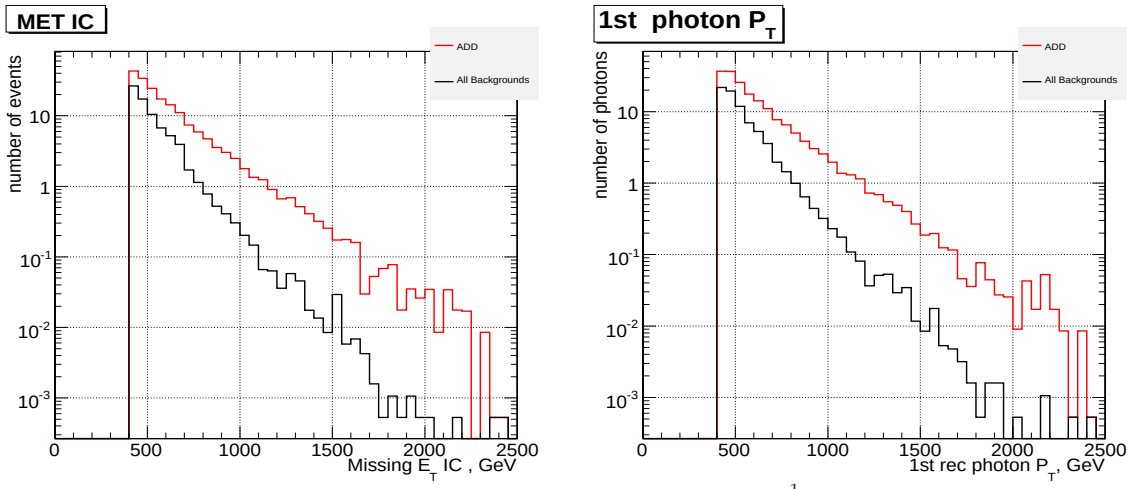

Figure 22: Signal and all backgrounds after all cuts normalised to $30\ \mathrm{fb}^{-1}$ for $\mathrm{M_D} = 2.5\ \mathrm{TeV}, n = 2$ ($\not{E}_T$ left, reconstructed photon p_T right).

Based on the calculated significances in table 18, the integrated luminosity necessary for a $5\,\sigma$ discovery can be calculated and is shown in table 19. If an ADD scenario with a low $\mathrm{M_D} < 3\ \mathrm{TeV}$ is realized in nature, a discovery would be possible even in the first years of the LHC data taking. Disentangling the number of extra dimensions however is going to be problematic. The reach of CMS to find extra dimensions in the graviton and photon channel for $30\ \mathrm{fb}^{-1}$ and $60\ \mathrm{fb}^{-1}$ is shown in figure 23 and figure 24.

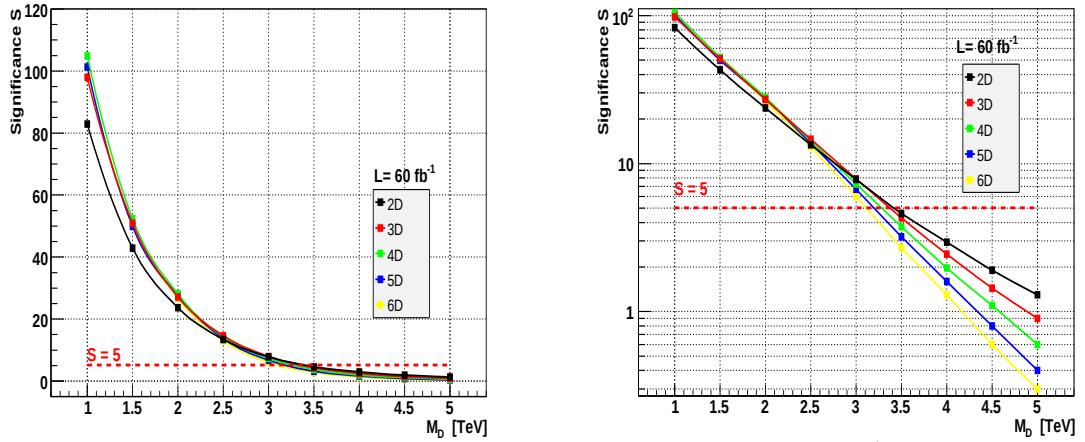

Figure 23: Signal and all backgrounds for $\not{E}_T$ after all cuts normalised to $60\ \mathrm{fb}^{-1}$ for $\mathrm{M_D} = 5\ \mathrm{TeV}, n = 2$.

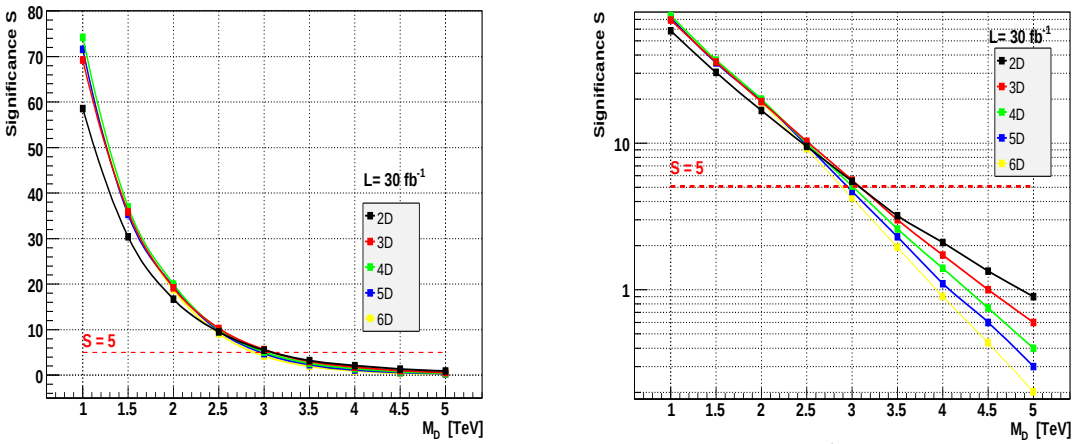

Figure 24: Signal and all backgrounds after all cuts normalised to 30 fb^{-1} for $\mathrm{M_D} = 2.5$ TeV, $n = 2$

$\mathrm{M_D}\,/n$	$n=2$	$n=3$	$n=4$	$n=5$	$n=6$
$\mathrm{M_D} = 1.0$ TeV	0.22 pb	0.75 pb	2.69 pb	10.07 pb	39.18 pb
$\mathrm{M_D} = 1.5$ TeV	43.81 fb	99.28 fb	0.23 pb	0.59 pb	1.52 pb
$\mathrm{M_D} = 2.0$ TeV	13.86 fb	23.56 fb	42.10 fb	78.64 fb	153.0 fb
$\mathrm{M_D} = 2.5$ TeV	5.67 fb	7.72 fb	11.03 fb	16.49 fb	25.67 fb
$\mathrm{M_D} = 3.0$ TeV	2.73 fb	3.10 fb	3.69 fb	4.60 fb	5.97 fb
$\mathrm{M_D} = 3.5$ TeV	1.47 fb	1.43 fb	1.46 fb	1.56 fb	1.74 fb
$\mathrm{M_D} = 4.0$ TeV	0.86 fb	0.73 fb	0.65 fb	0.61 fb	0.59 fb
$\mathrm{M_D} = 4.5$ TeV	0.54 fb	0.40 fb	0.32 fb	0.27 fb	0.23 fb
$\mathrm{M_D} = 5.0$ TeV	0.35 fb	0.24 fb	0.17 fb	0.12 fb	0.10 fb

Table 13: Total ADD cross section σ_{tot} for different $\mathrm{M_D}$, n parameter values.

M_D / n	$n = 2$	$n = 3$	$n = 4$	$n = 5$	$n = 6$
$M_D = 1.0$ TeV	26.46%	10.21%	3.23%	0.80%	0.23%
$M_D = 1.5$ TeV	49.34%	27.13%	12.15%	4.76%	1.95%
$M_D = 2.0$ TeV	68.48%	46.88%	27.62%	14.73%	7.24%
$M_D = 2.5$ TeV	81.50%	64.28%	44.09%	28.91%	17.16%
$M_D = 3.0$ TeV	89.74%	77.84%	60.68%	44.94%	30.61%
$M_D = 3.5$ TeV	94.53%	86.69%	73.46%	59.96%	45.26%
$M_D = 4.0$ TeV	97.22%	92.69%	83.48%	73.00%	60.55%
$M_D = 4.5$ TeV	98.74%	96.11%	90.62%	83.24%	73.88%
$M_D = 5.0$ TeV	99.40%	97.91%	94.85%	90.51%	83.61%

Table 14: Acceptance $\alpha(M_G)$ for signal events required to have $M_G < M_D$ in order to select only events from the region where the effective ADD theory is valid.

M_D / n	$n = 2$	$n = 3$	$n = 4$	$n = 5$	$n = 6$
$M_D = 1.0$ TeV	58.0 fb	76.5 fb	86.8 fb	80.5 fb	90.1 fb
$M_D = 1.5$ TeV	21.6 fb	26.96 fb	27.8 fb	28.0 fb	29.8 pb
$M_D = 2.0$ TeV	9.48 fb	11.0 fb	11.6 fb	11.1 fb	11.1 fb
$M_D = 2.5$ TeV	4.6 fb	4.97 fb	4.85 fb	4.77 fb	4.31 fb
$M_D = 3.0$ TeV	2.43 fb	2.38 fb	2.21 fb	2.07 fb	1.82 fb
$M_D = 3.5$ TeV	1.38 fb	1.23 fb	1.07 fb	0.93 fb	0.78 fb
$M_D = 4.0$ TeV	0.83 fb	0.67 fb	0.54 fb	0.44 fb	0.35 fb
$M_D = 4.5$ TeV	0.53 fb	0.39 fb	0.29 fb	0.22 fb	0.17 fb
$M_D = 5.0$ TeV	0.35 fb	0.24 fb	0.16 fb	0.11 fb	0.09 fb

Table 15: Effective ADD cross section after truncation for different M_D,n parameter values ($\sigma_{\text{eff}} = \sigma_{\text{tot}} * \alpha$).

M_D /n	$n=2$	$n=3$	$n=4$	$n=5$	$n=6$
M_D= 1 TeV	77.6 %	77.9 %	78.0 %	78.6 %	69.6 %
M_D=1.5 TeV	76.0 %	78.5 %	77.0 %	74.2 %	70.3 %
M_D=2 TeV	75.6 %	77.8 %	77.7 %	75.9 %	75.4 %
M_D=2.5 TeV	75.4 %	77.8 %	76.7 %	75.2 %	75.3 %
M_D=3.0 TeV	75.2 %	77.2 %	76.1 %	74.9 %	74.6 %
M_D=3.5 TeV	72.5 %	76.9 %	76.1 %	75.3 %	74.6 %
M_D=4. TeV	75.2 %	76.7 %	75.8 %	75.1 %	74.1 %
M_D=4.5 TeV	75.2 %	76.8 %	75.5 %	75.3 %	74.2 %
M_D=5. TeV	75.1 %	76.8 %	75.6 %	75.2 %	73.8 %

Table 16: Accepted ADD signal events after all cuts for different sampling points in the M_D, n space.

M_D / n	n =2	n=3	n=4	n=5	n= 6
$M_D = 1.0$ TeV	2726 /1363	3594/1797	4034/2017	3799/1899	3784/1892
$M_D = 1.5$ TeV	984/492	1267/633	1322/661	1232/616	1257/628
$M_D = 2.0$ TeV	430/215	514/257	541/270	526/263	501/250
$M_D = 2.5$ TeV	210/104	231/115	223/111	215/107	200/99
$M_D = 3.0$ TeV	110/55	111/56	102/51	92/46	82/41
$M_D = 3.5$ TeV	60/30	57/29	49/24	42/21	36/17
$M_D = 4.0$ TeV	37/19	32/15	25/12	20/10	16/8
$M_D = 4.5$ TeV	24/12	18/9	13/6	10/5	8/4
$M_D = 5.0$ TeV	16/8	11/5	7/3	5/3	4/2

Table 17: Number of expected events after an integrated luminosity of 60 fb^{-1} and 30 fb^{-1}.

$M_D\,/n$	$n=2$	$n=3$	$n=4$	$n=5$	$n=6$
$M_D = 1.0$ TeV	82.9/58.6	97.9/69.3	104.9/74.2	101.3/71.6	101.1/71.4
$M_D = 1.5$ TeV	42.9/30.4	50.9/35.9	52.3/37.0	49.9/35.3	50.6/35.8
$M_D = 2.0$ TeV	23.7/16.7	27.1/19.2	28.1/19.9	27.6/19.5	26.6/18.8
$M_D = 2.5$ TeV	13.4/9.5	14.6/10.4	14.2/10.0	13.7/9.7	12.9/9.1
$M_D = 3.0$ TeV	7.8/5.5	7.9/5.6	7.3/5.2	6.7/4.7	5.9/4.2
$M_D = 3.5$ TeV	4.5/3.2	4.3 /3.0	3.7/2.6	3.3/2.3	2.7/1.9
$M_D = 4.0$ TeV	2.9/2.1	2.4/1.7	1.9/1.4	1.6/1.1	1.3/0.9
$M_D = 4.5$ TeV	1.9/1.3	1.5/1.0	1.1/0.7	0.8/0.6	0.6/0.4
$M_D = 5.0$ TeV	1.3/0.9	0.9/0.6	0.6/0.4	0.4/0.3	0.3/0.2

Table 18: Significance $\mathrm{Sig} = 2(\sqrt{S+B} - \sqrt{B})$ after an integrated luminosity of 60 fb^{-1} and 30 fb^{-1}.

$M_D\,/n$	$n=2$	$n=3$	$n=4$	$n=5$	$n=6$
$M_D = 1.0$ TeV	0.21 fb^{-1}	0.15 fb^{-1}	0.13 fb^{-1}	0.14 fb^{-1}	0.14 fb^{-1}
$M_D = 1.5$ TeV	0.81 fb^{-1}	0.57 fb^{-1}	0.55 fb^{-1}	0.60 fb^{-1}	0.58 fb^{-1}
$M_D = 2.0$ TeV	2.6 fb^{-1}	2.0 fb^{-1}	1.8 fb^{-1}	1.9 fb^{-1}	2.1 fb^{-1}
$M_D = 2.5$ TeV	8.2 fb^{-1}	7.0 fb^{-1}	7.4 fb^{-1}	7.9 fb^{-1}	8.8 fb^{-1}
$M_D = 3.0$ TeV	24.4 fb^{-1}	24.0 fb^{-1}	28.1 fb^{-1}	33.3 fb^{-1}	41.9 fb^{-1}
$M_D = 3.5$ TeV	72.0 fb^{-1}	80.2 fb^{-1}	107.0 fb^{-1}	141.2 fb^{-1}	199 fb^{-1}
$M_D = 4.0$ TeV	173.0 fb^{-1}	249.0 fb^{-1}	387.8 fb^{-1}	581.3 fb^{-1}	904 fb^{-1}
$M_D = 4.5$ TeV	413.9 fb^{-1}	720.1 fb^{-1}	1310 fb^{-1}	2242 fb^{-1}	3884 fb^{-1}
$M_D = 5.0$ TeV	903.3 fb^{-1}	1846.2 fb^{-1}	4147 fb^{-1}	8183 fb^{-1}	16343 fb^{-1}

Table 19: Integrated luminosity necessary for a $5\,\sigma$ discovery.

7.2 Systematic uncertainties

The estimated significances can be affected by systematic uncertainties of the measurement. If we assume that the measurement of the photon p_T^γ in the electromagnetic calorimeter has an uncertainty of 2%, the cut efficiencies will be modified. In this case the background increases by 3.1 %, corresponding to 2.3 events. (The numbers of events given in this section as example always corresponds to 30 fb^{-1}.) We also investigated the effect on the significance by a miss-measurement of the $\not\!\!E_T$ assuming an uncertainty of 5 %. Under this assumption the background gets larger by 4.0 % or 3 events. Another source of systematic uncertainty originates from the parton distribution function (PDF): The parton distribution functions of interacting particles describe the probability density for partons undergoing hard scattering at the hard process scale and taking a certain fraction of the total particle momentum. In this study, all cross sections and samples were obtained using CTEQ6L. In order to estimate the cross section uncertainties originating from PDF uncertainties in this analysis the master equations were used:

$$\Delta X_1 = \frac{1}{2}\sqrt{\sum_{i=1}^{N}(X_i^+ - X_i^-)^2}\,;\ \Delta X_2 = \frac{1}{2}\sqrt{\sum_{i=1}^{2N} R_i^2} \tag{10}$$

$$\Delta X^+_{\mathrm{max}} = \sqrt{\sum_{i=1}^{N}[\max(\mathrm{X_i^+} - \mathrm{X_0}, \mathrm{X_i^-} - \mathrm{X_0}, 0)]^2}\,;\ \Delta X^-_{max} = \sqrt{\sum_{i=1}^{N}[\max(\mathrm{X_0} - \mathrm{X_i^+}, \mathrm{X_0} - \mathrm{X_i^-}, 0)]^2} \tag{11}$$

This leads to the following values :

$$W \to e\nu : \Delta X_1 = 7.81\%, \Delta X_2 = 8.64\%;\ \Delta X^+ = 8.47\%, \Delta X^- = 8.34\% \tag{12}$$

$$\gamma + Z \to \nu\bar{\nu} : \Delta X_1 = 7.92\%, \Delta X_2 = 8.81\%;\ \Delta X^+ = 8.13\%, \Delta X^- = 8.99\%. \tag{13}$$

If we assume the maximum uncertainty for these two main background components, the total background is increased by 7.5 % (5.6 events).
In conclusion, we have a total systematic error on the background of 9 %. The effect of the systematic error is shown in figure 25 and table 20, where the significances and the required luminosity for a 5 σ discovery are recalculated including systematics. On can see in table 20 that with this background uncertainty a discovery with 5 σ is not possible anymore above around 3.0. The calculation had been done using a program from the statistical webpage of Sergey Bityukov [15] to calculate significances including the estimated uncertainty on the background.

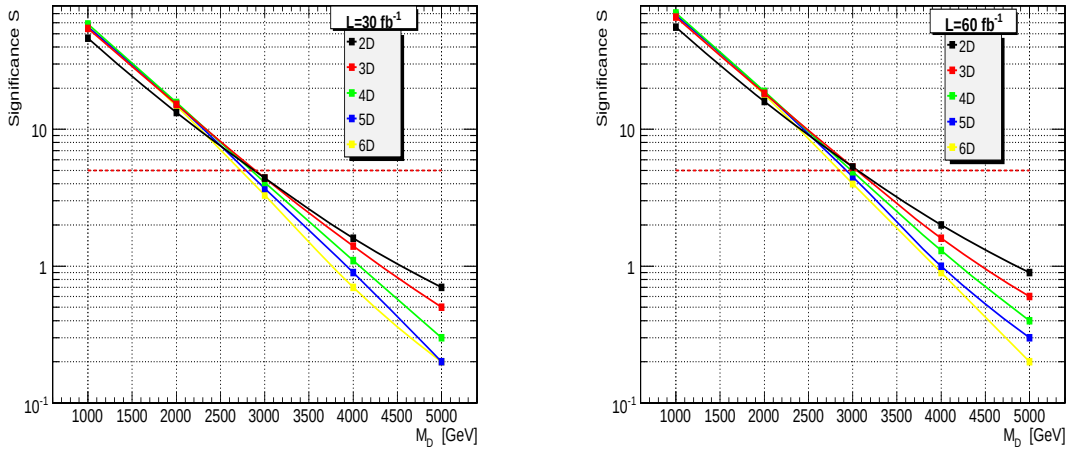

Figure 25: Signal and all backgrounds after all cuts normalised to 30 fb^{-1} for $\mathrm{M_D} = 2.5\ \mathrm{TeV}, n = 2$ including systematic uncertainties.

M_D / n	$n = 2$	$n = 3$	$n = 4$	$n = 5$	$n = 6$
$M_D = 1.0$ TeV	0.21 fb^{-1}	0.16 fb^{-1}	0.14 fb^{-1}	0.15 fb^{-1}	0.15 fb^{-1}
$M_D = 1.5$ TeV	0.83 fb^{-1}	0.59 fb^{-1}	0.56 fb^{-1}	0.61 fb^{-1}	0.59 fb^{-1}
$M_D = 2.0$ TeV	2.8 fb^{-1}	2.1 fb^{-1}	1.9 fb^{-1}	2.1 fb^{-1}	2.3 fb^{-1}
$M_D = 2.5$ TeV	9.9 fb^{-1}	8.2 fb^{-1}	8.7 fb^{-1}	9.4 fb^{-1}	10.9 fb^{-1}
$M_D = 3.0$ TeV	47.8 fb^{-1}	46.4 fb^{-1}	64.4 fb^{-1}	100.8 fb^{-1}	261.2 fb^{-1}
$M_D = 3.5$ TeV	**5 σ discovery not possible anymore**				

Table 20: Integrated luminosity necessary for a $5\,\sigma$ discovery including systematics. With a fundamental scale $M_D = 3.5$ TeV a $5\,\sigma$ discovery is not possible anymore.

8 Conclusion and outlook

Simulation studies of γ and $\not\!\!E_T$ as a signature for the discovery of ADD large extra dimensions with the CMS detector, have been performed. Signal samples for various model parameters as well as of possible backgrounds has been taken into account. The reconstruction performance and efficiency obtained with the fast simulation has been verified to compare with the detailed simulation, and has therefore been used for most parts of the analysis. A normalisation method is proposed to measure the main background $Z^0(\rightarrow \nu\bar{\nu}) + \gamma$ with high precision using reference rates and spectra from $Z^0(\rightarrow \mu\mu) + \gamma$ and $Z^0(\rightarrow ee) + \gamma$ that allows to control the background in the region of interest to about 5% after 10 fb^{-1}.

A $5\,\sigma$ discovery can be made with less than 1 fb^{-1} of data for scenarios with M_D in the range of 1-1.5 TeV, and less than 10 fb^{-1} for values of M_D in the range of 2-2.5 TeV, largely independent of the number of extra dimensions. These estimates are conservative taking into account only the events for which the graviton mass is smaller than M_D and should be considered as lower bound. The discovery reach for ADD extra dimensions via this channel with 60 fb^{-1} is about 3-3.5 TeV.

9 Acknowledgement

Thanks to Anja Vest and Filip Moortgat for technical and editorial help. Special thanks to Tanju Gleisberg for his SHERPA support.

References

[1] CMS Coll., "The Trigger and Data Acquisition project,Volume II", CERN/LHCC 2002-26,CMS TDR 6.2,15 December 2002.

[2] CMS Coll., Physics Technical Design Report, Volume 1, "Detector Performance and Software", CERN/LHCC 2006-001, CMS TDR 8.1, 2 December 2006.

[3] G.Grindhammer, M.Rudowicz and S.Peters, NIM A290(1990) 469, G.Grindhammer and S.Peters, hep-ex/0001020.

[4] Giudice, Gian F. and Rattazzi, Riccardo and Wells, James D. Quantum gravity and extra dimensions at high-energy colliders, hep-ph/9811291.

[5] OSCAR: CMS Simulation Package, see http://cmsdoc.cern.ch/oscar.

[6] ORCA: CMS Reconstruction Package, see http://cmsdoc.cern.ch/orca.

[7] FAMOS: CMS fast Simulation Package, http://cmsdoc.cern.ch/FAMOS .

[8] SHERPA, Theoretical high-energy physics research group
see http://www.sherpa-mc.de

[9] PAX: Physics Analysis eXpert,
see http://home.cern.ch/pax.

[10] CMKIN
see http://cmsdoc.cern.ch/cmsoo/projects/CMKIN.

[11] E. Meschi, T. Monteiro, C. Seez, and P. Vikas, Electron Reconstruction in the CMS Electromagnetic Calorimeter, CMS Note 2001/034 (June 2001).

[12] Nima Arkani-Hamed,Savas Dimopoulos and Gia Dvali, The Hierarchy Problem and New Dimensions at a Millimeter, 1998, hep-ph/9803315.

[13] B. Clerbaux, T. Mahmoud, C.Collard, M.-C. Lemaire, V. Litvin, TeV electron and photon saturation studies, CMS NOTE-2006/004.

[14] L. Vacavant, I. Hinchliffe, Signals of Models with Large Extra Dimensions in ATLAS, SN-ATLAS-2001-005.

[15] Statistical Webpage: Uncertainty, Systematics, Limits, ..., constructed and supported by Sergey Bityukov;
see http://cmsdoc.cern.ch/ bityukov.